SCIENTIFIC REPORTS

OPEN

Enhancement of superconducting properties and flux pinning mechanism on $Cr_{0.0005}NbSe_2$ single crystal under Hydrostatic pressure

S. Arumugam[1], Manikandan Krishnan[1], Kent Ishigaki[2], Jun Gouchi[2], Rukshana Pervin [3], G. Kalai Selvan[4], Parasharam M. Shirage[3] & Y. Uwatoko[2]

Superconducting properties of $Cr_{0.0005}NbSe_2$ (T_c~6.64 K) single crystals have been investigated through the temperature dependent resistivity (~8 GPa) and DC magnetization (~1 GPa) measurements. Further, the critical current density (J_c) as a function of applied magnetic field has been studied from magnetic isotherms. The vortex pinning mechanisms have also been systematically analyzed using weak collective pinning theory as a function of pressure. The J_c corresponds to the flux flow enhanced by the application of pressure due to increase of T_c and vortex changes. We found that the pressure is responsible for the spatial variations in the charge carrier mean free path (δl pinning). We find that core point pinning is more dominant than surface pinning which is caused by the application of pressure. In addition, $J_c(H = 0)$ increases from 3.9×10^5 (0 GPa) to 1.3×10^6 (1.02 GPa) A/cm^2 at 2 K as the pressure is increased from normal pressure to 1.02 GPa. The pressure dependence of T_c (dT_c/dP) becomes 0.91 K/GPa and 0.75 K/GPa from magnetization and resistivity measurements respectively. We found that the pressure promotes the anisotropy nature, and decrease of coherence length and resulting in pathetic interface of the vortex core with pinning centers.

Superconductivity in the transition metal dichalcogenides (TMDs) and their intercalated layered structure compounds have special features associated with extreme anisotropy of the superconducting materials[1]. Superconductivity and density waves are competing orders that derive from instabilities[2] due to internal and external perturbations such as chemical pressure, external pressure and magnetic field. Spontaneous formation of periodic lattice distortions and Charge Density Waves (CDW) could be thermodynamically favorable under certain conditions in low dimensional metals where the wave vector is generally known to depend on the nesting properties of the Fermi surface[3]. The symmetry breaking suggest that phonon−electron coupling usually occurs at certain transition temperature (T_{CDW}) and so called Peierls phase transition[2]. Recently, the TMDs are natural layered materials provided with a new platform to study superconductivity due to the tunable nature of the superconducting properties and coexistent with other collective electronic excitations as well as strong intrinsic spin-orbit coupling. The bulk crystals of TMDs are formed of monolayers and bound to each other by van der Waals attraction, which makes it feasible to investigate experimentally. Niobium diselenide ($NbSe_2$) is one of the most studied layered TMDs which has van der Waals attraction between the layers and it has generated much attention due to interplay of superconducting transition temperature (T_c)[4–7] and T_{CDW}[2,8–10] is around 7 K and 33 K respectively. Anisotropy in TMDs, particularly in $NbSe_2$ compounds, having the highest T_c among TMDs, could be significantly enhanced by introducing foreign atoms or molecules in the interlayer space (intercalation process)[6,9,11,12]. The intercalation ability of these compounds is related to the expected implementation of high temperature superconductivity in the sandwich type structures described by the excitonic mechanism[6,9,13]. Further remarkably, Zeeman-protected Ising superconductivity is expected in $NbSe_2$ due to non-centrosymmetric

[1]Centre for High Pressure Research, School of Physics, Bharathidasan University, Tiruchirappalli, 620024, India. [2]Institute of Solid State Physics, University of Tokyo, 5-1-5 Kashiwanoha, Kashiwa, Chiba, 277-8581, Japan. [3]Discipline of Metallurgy Engineering and Materials Science & Physics, Indian Institute of Technology Indore, Simrol Campus, Khandwa road, Indore, 453552, India. [4]Department of Physics, University of Alabama at Birmingham, Birmingham, AL, 35294, USA. S. Arumugam and Manikandan Krishnan contributed equally. Correspondence and requests for materials should be addressed to S.A. (email: sarumugam1963@yahoo.com)

structure with in-plane inversion symmetry breaking and strong spin-orbit coupling and the anomalous large in-plane critical magnetic field has become one important direction in crystalline 2D superconductors[11,12,14,15]. The vortex movement (i.e., vortex entry into or exit from a single-crystalline superconductor) is possibly pinned at the edges when applied very low magnetic field which can be generally attributed to the translational symmetry breaking at the edges and it is dependent on both shape and dimension of the superconductors[13,16]. The applied magnetic field would significantly modify the pinning and subsequently influence the magnetic behavior of the samples.

The TMDs superconductors have revealed wonderful superconducting properties including high values of T_c, critical current density (J_c), upper critical field (H_{c2}) and irreversible field (H_{irr}). In the presence of strong pinning, the vortex state of type-II superconductors is usually characterized by J_c that decreases monotonically with an increasing field (H) or temperature (T). In the weakly pinned superconductors, interplay between intervortex interface and flux pinning produces an unusual peak in J_c as a function of both field and temperature which are just below the normal-state boundary and it is usually designated as secondary peak effect[17,18]. Both strong pinning and high J_c depend on variation in the grain size and the coherence length (ξ)[19]. Vortex pinning arises from the interplay of several competing energies, namely the self-energy of the flux lines, vortex-vortex interactions, vortex inhomogeneity interactions and thermal excitations[20]. A magnetic field generates an array of vortices in type-II superconductors and the vortices strongly interact with each other forming highly correlated configurations such as the vortex lattice. In high-T_c cuprates at relatively high temperatures, vortices move and vibrate due to thermal fluctuations to the extent that the lattice can melt becoming a vortex liquid[21–23]. Growth of the structure of the vortex lattice in a weakly pinned high-T_c superconductor is of paramount importance, since it determines superconducting properties that are directly suitable for applications[24,25]. As the temperature is raised, the vortex lattice undergoes a first-order transition to a stable disordered state[24,26–28]. A thermal fluctuation permits pinned vortices to fluctuate around the potential energy and reduces the effective pinning energy due to thermal smearing. The vortices also escape totally from the pinning centers through a variety of de-pinning excitations. Vortex motion still occurs for currents lower than J_c at a much slower rate. This flux creep mechanism implies a residual dissipation and it is responsible for the time relaxation of persistent currents flowing in a superconducting closed loop.

Hydrostatic pressure effects on the T_c enhancement shows more advantages that are relevant to the flux pinning compared to other perturbations. The application of high pressure leads to changes in the electronic bands leading to original properties, which may be associated with a structural phase transition. It always reduces the lattice parameters and causes the shrinkage of unit cells, giving rise to the reduction of anisotropy. Grain connectivity improvement should also be expected, as pressure can compress both grains and grain boundaries. The formation of point defects can be more favorable under high pressure, since it is well known that the formation energy of point defects decreases with an increasing pressure. High pressure can cause low-angle grain boundaries to migrate in polycrystalline bulk samples, resulting in the emergence of giant grains, sacrificing surface pinning thereafter. Hence, a ratio of point pinning centers to surface pinning centers is expected to be higher due to an increase of formation energy under high pressure. Several examples can be recalled here. Pressure increases the superconducting transition from 3.5 K to 6.5 K and also the semiconducting to metallic transition in $LaO_{0.5}F_{0.5}BiS_2$ single crystals[29]. Whereas a large enhancement of T_c from 26 K (0 GPa) to 43 K (4 GPa) in $LaO_{0.95}F_{0.05}FeAs$[30] with application of external hydrostatic pressure up to 3 GPa using piston cylinder pressure device, T_c was reduced with the application of pressure above 3 GPa to 30 GPa, using a diamond anvil pressure device. Further, pressure induced superconductivity has been observed in the pnictides such as $LaFeAsO_{1−x}F_x$, $LaFePO$ and $SrFe_2As_2$[31]. In the ladder compounds, pressure induces the metal-insulator transition generating hole carriers and eventually superconductivity occurs in $Ca_{14−x}Sr_xCu_{24}O_{41}$[32]. Pressure is also an effective approach to improve the J_c significantly in $FeSe$[33], $Sr_4V_2O_6Fe_2As_2$[34] $YBa_2Cu_3O_{7−x}$[35] superconductors, as the pressure induces more point pinning centers and subsequently affects the pinning mechanism[33,34]. The investigation of the pressure dependence of thermodynamic magnitudes proved to be a useful method of studying the properties of anisotropic compounds. Such investigations were performed on the layered compound $NbSe_2$[36–39]. Pressure not only enhanced T_c with a rate of dT_c/dP is 0.86 K/GPa ($NbSe_2$) and 1.47 K/GPa ($Fe_{0.0011}NbSe_2$) but also increased J_c and H_{c2}[38]. In the case of the intercalated $NbSe_2$ pressure increased T_c and simultaneously suppressed T_{CDW}[40]. Suderow et al., described the pressure dependence of anisotropy, of the electron-phonon coupling and Fermi velocities, which influence the peculiar interplay between CDW, Fermi surface complexity and superconductivity in $NbSe_2$[41]. Pressure induces a transition from spatial variation in the δT_c pinning to $\delta\ell$ pinning mechanism in the undoped $NbSe_2$ superconductors[38].

From above, it is clear that high pressure is exclusively unique in fine-tuning superconducting states with the benefit of without introducing disorder effects in comparison with chemical doping. High pressure is, thus, an important tool to study intrinsic properties of the materials to understand the enhancement of T_c, J_c and other physical properties[23,33,34,36,38,40,42–44]. These facts motivated our present study on the pressure effects on the superconducting properties of single crystalline Cr_xNbSe_2. We anticipated that hydrostatic pressure would increase the superconducting volume, H_{irr}, and H_{c2} due to enhancement of T_c, increase the point defect and reduction in the anisotropy of single crystalline Cr intercalated $NbSe_2$ samples. Indeed, we observed such interesting properties when pressure was applied to Cr intercalated $NbSe_2$ is investigated. These findings are reported below.

Results and Discussions

The temperature dependence of resistivity ($\rho(T)$) in the temperature range from 2 to 300 K under various hydrostatic pressures from 0 to 8 GPa [Fig. 1(a)], the expanded region near T_c [Fig. 1(b)] and zero-field-cooled (ZFC) and field-cooled (FC) dc magnetization ($M(T)$) at the constant magnetic field of 20 Oe [Fig. 1(c)] in the vicinity of the T_c under various hydrostatic pressures range from 0 to 1 GPa of the crystal flakes of $Cr_{0.0005}NbSe_2$ are shown respectively in Fig. 1(a,b and c). The T_c is defined as an onset, mid and offset of superconductivity with obtained
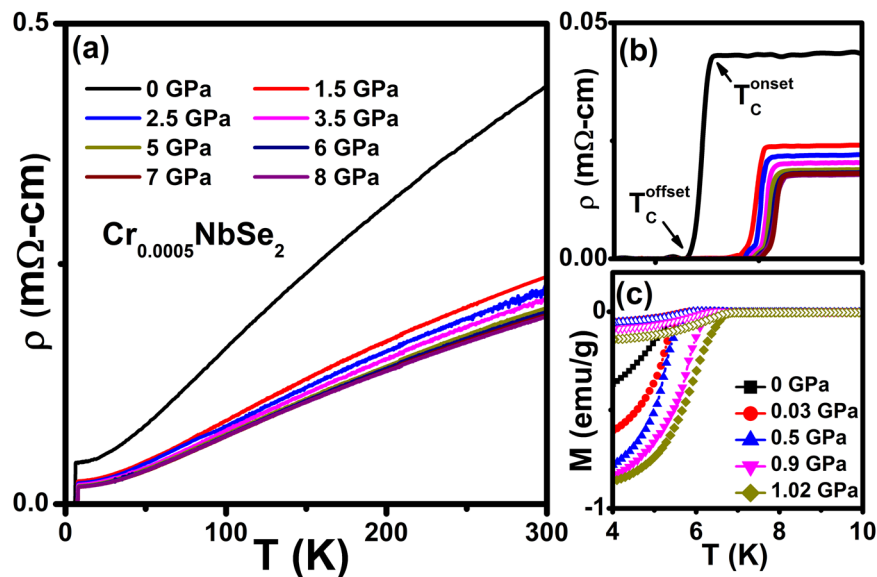
Figure 1. (**a**) Temperature dependent of resistivity at various applied hydrostatic pressures from 0 to 8 GPa, (**b**) pressure evolution of onset (T_c^{onset}) and offset (T_c^{offset}) superconducting transition temperature from resistivity measurements c) temperature dependent of zero field cooled (ZFC) [closed symbols] and field cooled (FC) [open symbols] dc magnetization at various hydrostatic pressures from 0 to 1.02 GPa.

from dR/dT in $\rho(T)$ measurements and the onset of diamagnetic signals corresponds to superconductivity as observed from $M(T)$ measurements. As shown in Fig. 1(a), the ρ decreases (0.44 to 0.04 mΩ-cm at 0 GPa and 0.20 to 0.018 mΩ-cm at 8 GPa) in the temperature region from 300 to 10 K. It is also clear from Fig. 1(c), that $M(T)$ starts to deviate from the normal state behavior around 6.1 K due to the presence of a diamagnetic signal, which is slightly above the onset of T_c. The sharp superconducting transition along with the large residual resistivity ratio (~11) and superconducting width ($\Delta T_c = T_c^{onset} - T_c^{offset}$) indicate good quality of single crystals used in the present study. The observation of sharp superconducting transition and zero resistivity at each applied pressure ensure indicate the hydrostatic nature in our experiments. As shown in Fig. 1(a), normal state resistivity gradually decreases with the application of high pressure and it almost shows the metallic nature for all pressures up to ~ 8 GPa. Similar $\rho(T)$ behavior under pressure has been reported for various superconducting materials[33,34,36,38,40]. This is associated with the fact that high pressure brings the layers in the unit cell closer together, and facilitates overlap of wave functions of the conduction electrons in the adjacent layers. The T_c (6.64 K) of $Cr_{0.0005}NbSe_2$ is found to be less than undoped $NbSe_2$ single crystal, and similar trend has been reported for various intercalated compounds Fe_xNbSe_2[6,38], $NbSe_2$[36,40], Ga_xNbSe_2[11], Pd_xNbSe_2[45], Cu_xNbSe_2[12], $(LaSe)_{1.14}(NbSe_2)$[46] pnictides[34,44] at both ambient and pressure.

Figure 1(c) shows $M(T)$ in the ZFC and FC regimes with an applied magnetic field of 20 Oe under various hydrostatic pressures up to ~ 1 GPa in the vicinity of T_c up to 10 K; We clearly notice the diamagnetic transition at 6.14 K and 7.07 K at ambient and 1.02 GPa respectively. The diamagnetic transition shifts towards high temperature with the application of pressure as shown in Fig. 2(a). The hysteresis between ZFC and FC regimes indicates that $Cr_{0.0005}NbSe_2$ exhibits weak flux pinning centers. Without correcting the demagnetization factor, we estimate the superconducting volume fraction (ZFC) to be ~ 80% indicative of bulk superconductivity. At ambient pressure the sample shows a T_c of 6.14 K from $M(T)$ at constant magnetic field of 20 Oe and it is ~0.5 K less than that observed from $\rho(T)$ measurements, as shown in Fig. 2(a). Evidently, T_c^{onset} and T_c^{offset} observed from $\rho(T)$ is higher than $M(T)$ measurements as shown in Fig. 2(a). With the application of high pressure, T_c onset steadily increases in entire pressure region due to the reduction of interlayer distances of $Cr_{0.0005}NbSe_2$ as shown in Fig. 2(a).

With an application of pressure, the room temperature resistivity (ρ^{300K}) decreases monotonically up to 8 GPa and favours enhancement of metallic nature [Fig. 1(a)]. However, ρ^{300K} decreases at a faster rate (0.13 mΩ-cm/GPa) up to 1.5 GPa and then moderate decrease (0.01 mΩ-cm/GPa) is observed above 1.5 GPa to 8 GPa. Further, $\rho^{T_c(onset)}$ decreases with slower rates are 0.01 mΩ-cm/GPa and 0.001 mΩ-cm/GPa at below and above 1.5 GPa respectively. Hence, we found that both ρ^{300K} and $\rho^{T_c(onset)}$ are sensitive to the low pressure as shown in Fig. 2(b). $\rho(T)$ is found to be almost linear in the high temperature region for various applied pressures. The change in $\rho(T)$ shows metallic behavior at all pressures of up to 8 GPa. The upward curvature in $\rho(T)$ weakens progressively with increasing pressure. Figure 2(a) shows the rapid enhancement of T_c in the low pressure region and moderate increase in high pressure region as we observed from both $\rho(T)$ and $M(T)$ for $Cr_{0.0005}NbSe_2$. One can see that the both T_c^{onset} and T_c^{offset} shift towards higher temperature with the application of high pressure and the dT_c/dP becomes 0.91 K/GPa in the $0 < P < 1$ GPa from $M(T)$ measurements. The rate of change of T_c with pressure $dT_c/dP = 0.75$ K/GPa for P less than 1.5 GPa and 0.09 K/GPa in the interval $1.5 < P < 8$ GPa as observed from $\rho(T)$ measurements. These results suggest that the relative change in the density of states at the Fermi level is profound in low pressure region up to 1.5 GPa and the moderate increase in the high pressure region ($1.5 < P < 8$ GPa)
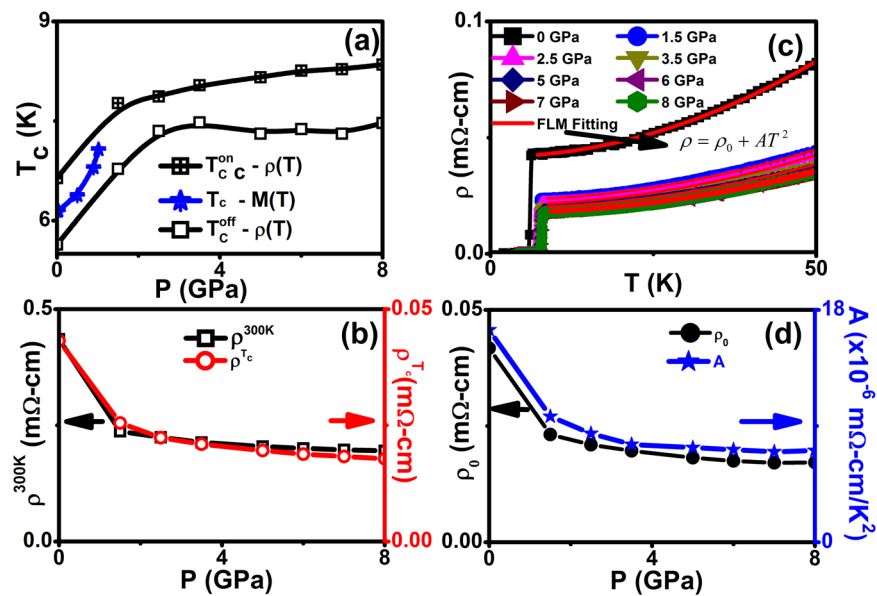
Figure 2. (**a**) Pressure dependent of superconducting transition temperature (T_c) from resistivity and magnetization measurements, (**b**) pressure dependent of resistivity of T_c^{onset} (ρ_c^T) and room temperature (ρ^{300K}), (**c**) excellent fitting to the resistivity data from 7 to 50 K using Fermi-liquid model ($\rho = \rho_0 + AT^2$) for various pressures, and (**d**) pressure dependent of residual resistivity (ρ_0) and scattering factor (A) from FLM fitting for $Cr_{0.0005}NbSe_2$.

which leads to corresponding variation of T_c. This is associated with the fact that the P brings the layers closer together, and it facilitates the overlap of the wave functions of the conduction electrons in the adjacent layers. Consequently, an increase in T_c is mainly determined by changes in the density of states at the Fermi level and the change in the phonon spectrum plays a minor role. The region above 100 K in $Cr_{0.0005}NbSe_2$ can be described reasonably well by straight line fits with different slopes for various pressures in $\rho(T)$ suggesting that phonon scattering mechanism is dominant.

The relationship between interlayer spacing and T_c is a matter of fundamental importance in understanding of superconductivity in layer compounds. The effect of pressure upon the physical properties is due to the reduction in interlayer spacing. The band structure calculations of the Fermi level for $NbSe_2$ at the middle of a narrow d sub-band situated between the unoccupied and primarily d bands of Nb and the fully occupied p bands of Se. Although differing in the details of the sub-band overlap with the p bands, both calculations highlight the importance of interband (hybridization) and interlayer interactions. These take the form of a nonzero empty site potential at the unoccupied interstitial positions between the Se layers due to wave function overlap in the modified muffin tin potential approach of Kasowski[47]. From earlier report, we inferred that neglecting a weak empty site potential broadens the sub-band and increases the overlap with the p bands. If the charge transfer occurs due to intercalation, shifts in the Fermi level towards the sloped region of the density of states curve and this can lead to a relatively a big change in density of states ($N(\varepsilon_F)$) under pressure, and consequently, in T_c. More detailed information about the electronic properties and superconductivity of the pure and intercalated $NbSe_2$ solid solution was obtained from specific heat[12] measurements.

The phonon mediated superconductors, the electron-phonon coupling constant have been estimated from McMilllan formula[48] using Debye temperature[49] and T_c,

$$T_c = \frac{\theta_D}{1.45}\exp\left(-\frac{1.04(1 + \lambda)}{\lambda - \mu(1 + 0.62\lambda)}\right),$$

where θ_D is the Debye temperature, μ^* is the screened pseudo-potential (characteristic for the electron repulsion) and assumed to be 0.15 suggested by McMilllan[48] for transition metallic superconductors and λ is the electron-phonon coupling constant and the parameters θ_D, μ^* and λ are all pressure dependent. The values of λ is 0.84 at ambient pressure suggest that strong coupling in superconductivity. With the Sommerfeld parameter (γ) and the electron-phonon coupling constant (λ), the electron density of states at the Fermi level ($N(\varepsilon_F)$) can be obtained from $N(\varepsilon_F) = 3\gamma/\pi^2 k_{B^2}(1 + \lambda)$. The density of electronic states at the Fermi energy therefore clearly decreases when more metal ions intercalates into $NbSe_2$. All the values of θ_D and $d\theta_D/dP$ for pure and intercalated samples are identical. The pressure dependence of Debye temperature $\theta_D(P)$ can be obtained from the Gruneisen's formula[48], $\frac{1}{\theta_D} = \frac{\partial\theta_D}{\partial P} = \frac{\alpha V}{C_V}$, where α is the thermal expansion coefficient, C_v is the heat capacity and the value of $d\theta_D/dP$ is one order of magnitude lower than the corresponding changes is T_c with pressure. The large relative growth of T_c can be qualitatively associated with the particularities of the $NbSe_2$ band structure, and corresponding changes of $\lambda(P)$[40]. Earlier it was shown that the intercalated Fe and Cu is located in the interlayer space, when the superconducting properties are affected by the interlaminar intercalant[12]. A redistribution of the interlayer
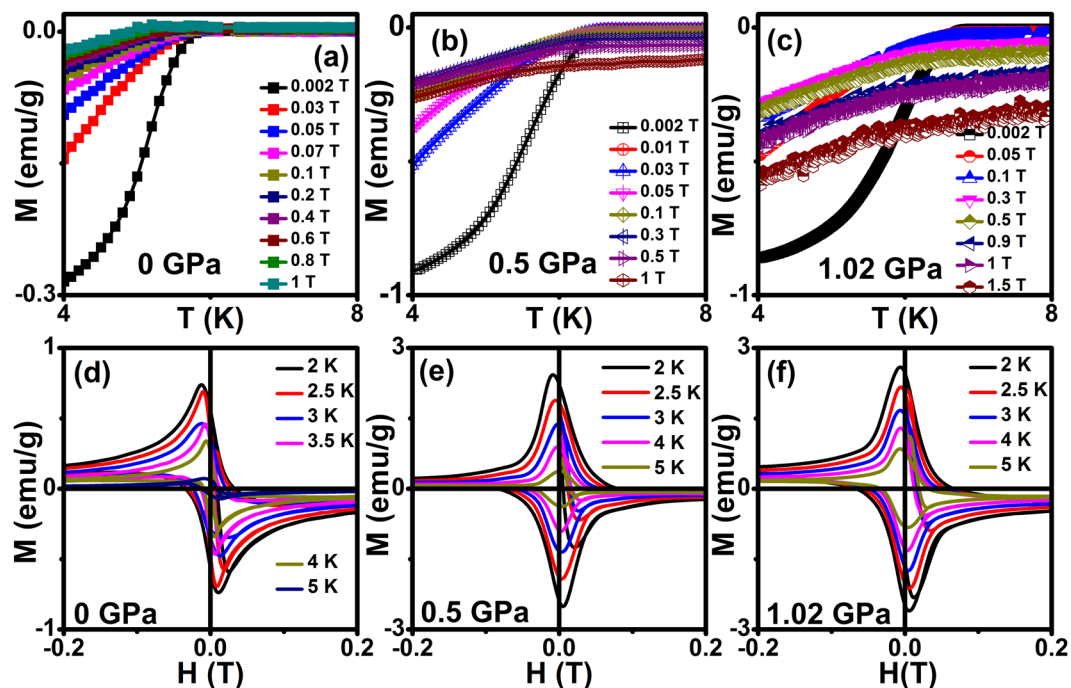
Figure 3. (**a**), (**b**) and (**c**) Temperature dependent of dc magnetization at various magnetic fields for 0, 0.5 and 1.02 GPa respectively on $Cr_{0.0005}NbSe_2$, (**d**), (**e**) and (**f**) Field dependent of magnetization scan in a low field range ($dH/dt \sim 20\,Oe/s$) at various temperatures for 0 GPa, 0.50 GPa & 1.02 GPa respectively on $Cr_{0.0005}NbSe_2$.

under pressure can serve as an additional reason for the changes in T_c[39]. The last idea is supported by an increase of the width of the superconducting transition under pressure and more pronounced manifestation of its stepped form. This type of evolution in the superconducting state under high pressure[38,44,50] has been observed in layered structure superconductors with a small anisotropy parameter[23,33,34].

It is known that T_c is found to increase for $NbSe_2$[12,39], Fe_xNbSe_2[38] and $Cr_{0.0005}NbSe_2$ compounds by applying high pressure. Figure 2(c) examines the normal-state resistivity of $Cr_{0.0005}NbSe_2$ under hydrostatic pressure and its implication of electronic correlation. Low temperature region ($7 \leq T \leq 50\,K$) of $\rho(T)$ can be fitted using the Fermi liquid model, $\rho = \rho_0 + AT^2$, where ρ_0 is residual resistivity and A is a scattering factor. Figure 2(c) shows good fitting for both data at ambient and high pressure and it supports the Fermi liquid model. The value of ρ_0 is 0.042 mΩ-cm: 0 GPa and 0.017 mΩ-cm (8 GPa) and the A [16.45×10^{-6} mΩ-cm/K^2 (0 GPa) and 7.1×10^{-6} mΩ-cm/K^2: 8 GPa] value shows clear indication of electron-electron interaction exhibits in both ambient and high pressure in this sample. The nature ρ_0 and A under various hydrostatic pressure has been shown in Fig. 2(d) which suggests that $Cr_{0.0005}NbSe_2$ is a weakly correlated system.

Figure 3(a–c) [Fig. S2] shows the temperature dependent of dc magnetization with various applied magnetic fields (*H*) with the constant *P* of 0, 0.5 and 1.02 GPa respectively. It is found that both T_c and diamagnetic signal show decreasing trend and allows us to determine the upper critical field (H_{c2}) of this material at various pressures. Taking the onset of transition in $M(T)$ at various magnetic fields with constant pressure as the upper critical field point $H_{c2}(T_c)$ and infer that almost all Cooper pairs are broken at this temperature and *H*. Further, the Meissner signal is suppressed with the application of various *H* at 0 GPa. However, the Meissner signal enhances at various *H* with constant pressure of 0.5 and 1 GPa, and it confirms that the pinning centers increase due to the application of pressure. Figure 3(d–f) shows the field dependent isothermal magnetization (MHL) scan in a low field region under various temperatures with applied pressure of 0, 0.5 and 1 GPa respectively. These results reveal that magnetic moment increases with the application of constant pressure, and confirms that when the occurrence of pinning increases as pressure increases in the sample.

According to the Ginzburg–Landau (GL) theory, the absolute zero temperature upper critical field $H_{c2}(0)$ can be estimated by using formula, $H_{c2}(T/T_c) = H_{c2}(0)(1 - [T/T_c]^a)^b$ with a = 1.39 and b = 1 associated with the large gaps that open in the Nb bands[51] which gives values less than that observed from WHH approach and the values $H_{c2}(0)$ [Fig. S1] are shown in Table 1. The orbital limited upper critical fields [$H_{c2}^{orb}(0)$] are estimated using the Werthamer–Helfand–Hohenberg (WHH)[52] empirical formula, $H_{c2}^{orb}(0) = -0.693 T_c (dH_{c2}/dT)_{T=T_c}$ and these values are shown in Table 1. For the Superconducting materials exhibiting weak coupling case, the Pauli limited upper critical field is calculated from, $H_p(0) = 1.84 T_c$, where T_c is taken from $M(T)$ measurements and the values are shown in Table 1. $H_p(0)$ indicating that both orbital effect and Pauli spin paramagnetic effect (PSP) which gives an influence on the pair-breaking mechanism through the entire pressure region. However, we haven't excluded the effect of spin instability at low temperatures, which may very well play an important role in the occurrence of superconductivity. The absolute orbital upper critical field $H_{c2}^{orb}(0)$ [Fig. S1] destroys superconductivity characteristics by enhancing the pair breaking phenomena in the presence of magnetic field and the values

P (GPa)	$H_p(0)$ (T)	$H_{c2}^{orb}(0)$ (T)	$H_{c2}(0)$ (T)	$\xi_{GL}(0)$ (nm)	$H_{c1}^{'}(0)$ (T)	$\lambda(0)$ (nm)
0	11.30	5.89	4.81	8.73	0.051	80.4
0.5	11.79	9.68	7.53	6.50	0.159	59.2
1.02	12.36	10.27	9.39	5.82	0.178	56

Table 1. Summary of the upper and lower critical field for the $Cr_{0.0005}NbSe_2$ single crystal under pressure.
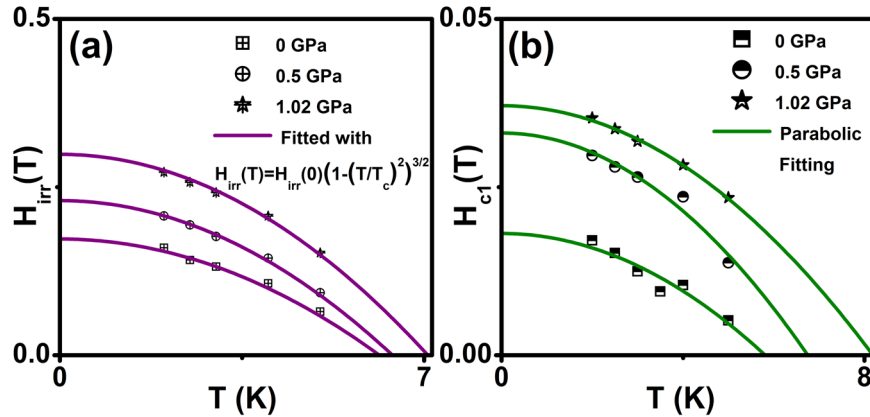

Figure 4. (**a**) Temperature dependence of irreversible field (H_{irr}) for $Cr_{0.0005}NbSe_2$ sample under pressure. Solid lines represent how fit the relation $H_{irr}(T) = H_{irr}(0)(1 - (T/T_c)^2)^{3/2}$, (**b**) shows the lower critical field (H_{c1}) for $Cr_{0.0005}NbSe_2$ sample under pressure. Solid lines show the parabolic fitting.

of $H_{c2}^{orb}(0)$ are found to be higher at higher pressures than at ambient pressure. Further, the enhancement of critical field under pressure implies that the strong flux pinning exhibits in this sample. Since, Pauli limit superconductivity mechanism [$H_{c2}(0) < H_{c2}^{orb}(0) < H_p(0)$] is exhibited by this sample, the calculated Maki parameter $\alpha = \sqrt{2}H_{c2}^{orb}(0)/H_p(0)$, is found to be nearly 1 at both ambient and at high pressures. Similar pressure dependences of $H_{c2}(P)$ were reported in YBCO[42], FeSe[43] Fe_xNbSe_2[38] indicating clearly that pressure influences the upper critical field. The superconducting coherence length [$\xi_{GL}(0)$] can be estimated from the relation, $\xi_{GL}(0) = [\Phi_0/2\pi H_{c2}(0)]^{0.5}$ where $\Phi_o = 2.07X10^{-7}G-cm^2$ and the values of $\xi_{GL}(0)$ are calculated from ambient and high pressure and it is shown in Table 1.

The irreversible field (H_{irr}) is calculated from MHL using the criteria of the zero field current density [$J_c(H=0)$] and it occurs due to depinning of the magnetic fluxes in this sample. Figure 4(c) shows temperature dependent of H_{irr} fitted with the equation, $H_{irr}(T) = H_{irr}(0)(1 - (T/T_c)^2)^{3/2}$, pressure up to ~ 1.02 GPa. It reveals that enhancement of H_{irr} with application of pressure and also provides evidence of the 3D nature of flux creep in the sample. This is an indication that H_{irr} is mainly controlled by the flux pinning. H_{c1} is measured from MHL under various temperatures [Fig. 3(a–c)] and plotted as a function of temperature with the parabolic function fitting as shown in Fig. 4(d). The precise determination of $H_{c1}(0)$ from MHL possibly suffers from demagnetization effect. Further, $H_{c1}(0)$ can also be deduced from the first penetration field $H_{c1}^{'}(0)$, assuming that the magnetization $M = -H_{c1}$, when the first vortex enters into the sample. Thus, magnetic field has rescaled to $H_{eff} = H - NM$ and $H_{c1}(0) = H_{c1}^{'}(0)/(1 - N)$, where N is a demagnetization factor and H is a magnetic field. It has been shown by Brandt[53] that a bar sample with a rectangle cross-section, the effective demagnetization factor $N = 1 - \tanh\sqrt{0.36t/b}$, where b and t width and thickness of the sample. Using this criterion, $H_{c1}(0)$ was estimated and fitted to the parabolic temperature dependence $H_{c1}(T) = H_{c1}(0)(1 - (T/T_c)^2)$ and the experimental $H_{c1}(0)$ is estimated at various pressures. The fit of our data to this expression (solid red line) suggests that vortex penetration in this material can be well described by BCS theory. Although the demagnetization effect is small and corrected lower critical field $H_{c1}^{'}(0)$ is calculated from $H_{c1}(0)$ with demagnetization correction using Brandt's formula, $H_{c1}^{'}(0) = H_{c1}(0)/\tanh\sqrt{0.36t/b}$ for approximate slab geometry[53] and these values of $H_{c1}^{'}(0)$ listed in Table 1. Using the $H_{c1}(0)$, it is possible to estimate the penetration depth from the relation, $\lambda(0) = [(\Phi_0/2\pi H_{c1}^{'}(0))(\ln\kappa + 0.5)]^{0.5}$, where $\lambda(0)$ is the penetration depth at 0 K. The ratio between the $\lambda(0)$ and coherence length ($\xi_{GL}(0)$ gives GL parameter (κ) through the expression $\kappa = \lambda(0)/\xi_{GL}(0)$. The value of $\kappa = \sqrt{1/2}$ has been conventionally used to classify superconductors as type I or type II based on whether κ value is higher or lower than $\sqrt{1/2}$. Our analysis predicts that κ value is very much higher than critical value and indicates $Cr_{0.0005}NbSe_2$ as a type II superconductor. Similarly Cu_xNbSe_2[12] and $Zr_{0.96}V_{0.04}B_2$[54] compounds were shown to be type-II superconductor, since κ value has been reported larger than the critical value.

Figure 5(a–d) shows the field dependence of superconducting critical current density ($J_c(H)$) on $Cr_{0.0005}NbSe_2$ for various temperatures at constant hydrostatic pressures of 0, 0.03, 0.5, 0.90 and 1.02 GPa. The $J_c(H)$ is estimated from MHL using Bean's model[55,56] $J_c = 20\Delta M/(b(3l-b)/3l)$, where width of the magnetization [$\Delta M = M^+(H) - M^-(H)$], b is a width and l is a length of the samples ($b < l$) were in mm. In general,
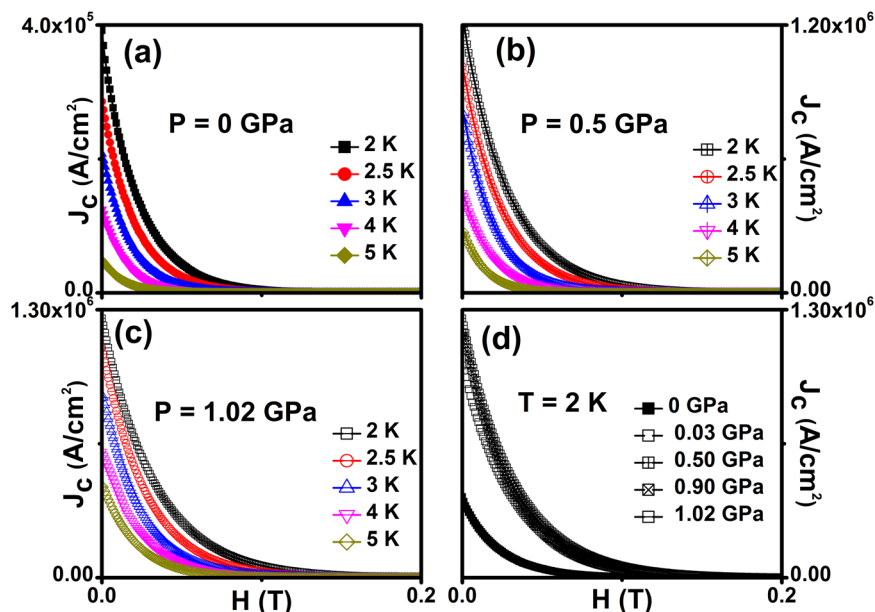
Figure 5. (**a**), (**b**), (**c**) and (**d**) Magnetic field dependent critical current density (J_c(H) on $Cr_{0.0005}NbSe_2$ for various hydrostatic pressures at various temperatures.

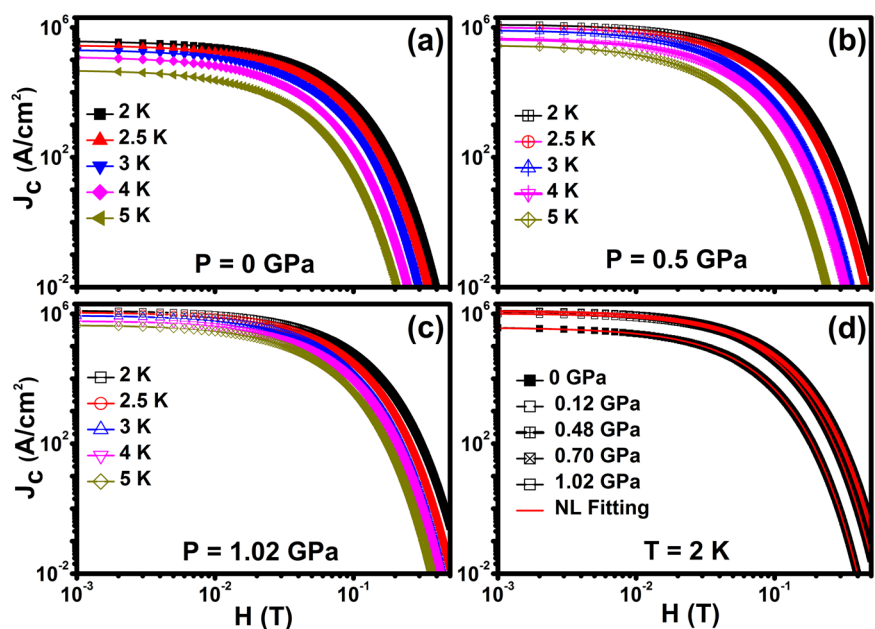**Figure 6.** (**a**), (**b**), (**c**) and (**d**) Logarithmic scale of magnetic field dependent superconducting critical current density J_c(H) on $Cr_{0.0005}NbSe_2$ for various temperatures and a few fixed hydrostatic pressures. Solid lines are shown in the collective pinning model fitting at the log scale at a temperature of 2 K.

low-magnetic field region, the gap ΔM in magnetization loop is mainly caused by the intergranular current. However, in the high-field region, ΔM results largely due to the intragranular current. Similar results have been reported from *M(H)* measurements on cuprates[57] and pnictides[58,59].

High pressure enhances the J_c in $Cr_{0.0005}NbSe_2$ sample and subsequently enhances flux pinning with an increase of point pinning centers. The J_c(0) values determined from MHL curves at 2 K are 391884, 1029067, 1190414, 1169989, 1258268 A/cm^2 for 0, 0.03, 0.5, 0.9 and 1.02 GPa respectively and the J_c(H = 0) increased by a factor of three at higher pressures. Figure 6(a–c) shows J_c(H) [Fig. S3] in the logarithmic scale for various temperatures and reveals that J_c exponentially decreases as the H increases. This result indicates that occurrence of weak pinning singularities, since magnetic impurities (Cr) act as point pinning centers. Further Fig. 6(d) shows exponential decay of J_c with an increase in applied magnetic field and these results compared theoretically, $J_c(H) = J_c(0) \exp\{-(H/H_0)^{3/2}\}$ and found excellent fitting for various pressure and temperatures.
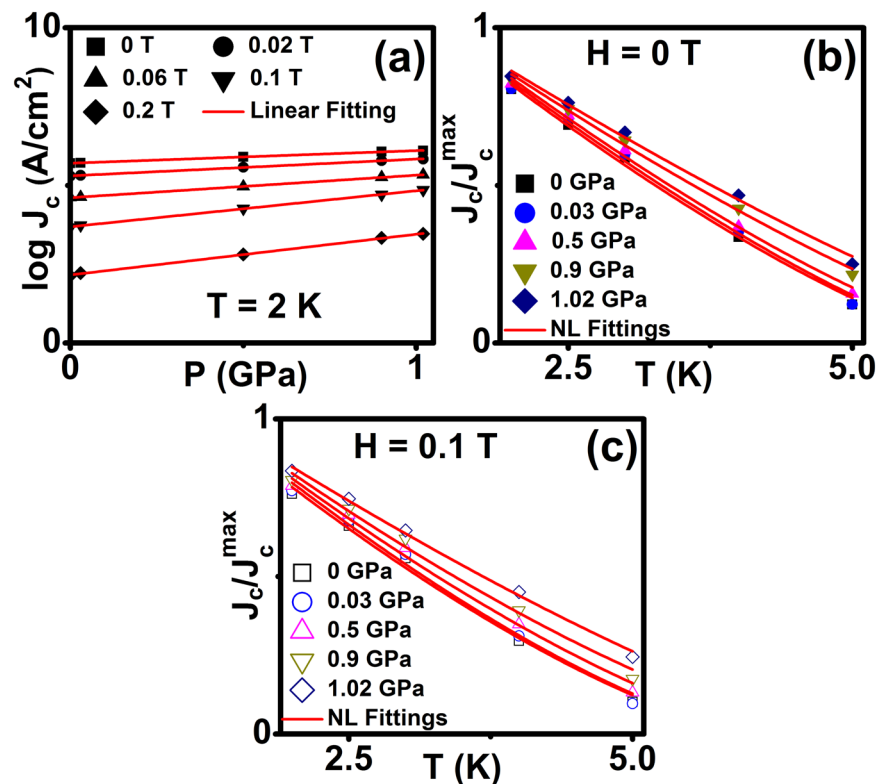
Figure 7. (**a**) Pressure dependence of J_c at 0, 0.02, 0.06, 0.1 and 0.2 T for 2 K. Solid lines are shown in the Linear fitting, (**b**) and (**c**) Temperature dependent normalized J_c at various pressures for constant magnetic field of 0.05 and 0.1 T. Solid lines are shown in the $J_c \propto (1 - T/T_c)^n$ fitting.

Figure 7(a) shows J_c as a function of pressure in logarithmic scale at 2 K under various fields and the solid lines show linear fits to the data, which gives the slopes [d(logJ_c)/dP] of 0.40, 0.53, 0.71, 1.14 and 1.29 GPa^{-1} at 0, 0.02, 0.06, 0.1 and 0.2 T respectively. These results indicate that application of pressure leads to an enhancement in J_c and it is more significant at higher fields. The normalized J_c as a function of temperature at 0 and 0.1 T for various pressures is shown in Fig. 7(b,c) and fitted with the scaling relation $J_c \propto (1 - T/T_c)^n$ where n is the critical exponent at each pressure. It is known that GL theory predicts distinct vortex pinning mechanisms in superconducting materials, with different values of exponent (n) at specific fields. The value of $n = 1$ and $n > 1.5$ corresponds to non-interacting vortices and strong vortex core pinning mechanism respectively. The critical exponent is estimated from fitting the scaling relation in Fig. 7(b,c) for various magnetic fields at constant hydrostatic pressure. It reveals that the values of n are found to be $1.65 \leq n \leq 2.12$ (0 T) and $2.82 \leq n \leq 3.75$ (0.1 T) under various hydrostatic pressure and shows higher value of n under pressure than at ambient pressure. Similar behaviour has been reported on $J_c(P)$, $J_c(T)$ and vortex dynamics properties in Fe$_x$NbSe$_2$[38] and in pnictides[34].

The core pinning mechanism is examined in the framework of collective pinning theory in this sample. Generally, core pinning comprises that pinning mechanism related to the spatial variation in the charge carrier mean free path (l), called δl pinning and pinning due to randomly distributed spatial variation in T$_c$, called δT_c pinning, which is mostly due to crystal defects[60]. We analyzed the pinning mechanism as reported by Griessen *et al.*[60] using the relation $J_c/J_0 \propto (1 - t^2)^{5/2}/(1 + t^2)^{1/2}$ for δl pinning mechanism, while $J_c/J_0 \propto (1 - t^2)^{7/6}/(1 + t^2)^{5/6}$ applies to δT_c pinning, where $t = T/T_c$. Figure 8(a–f) shows almost perfect matching of the experimentally obtained J_c with the theoretically calculated values and favour δl pinning mechanism in the entire pressure region. Our analysis directly supports δl pinning mechanism whatever be the pressure, and it is responsible for increasing in T_c Our results suggest that there is a single vortex pinning due to spatial variations in the charge-carrier mean free path. The coherence length is proportional to the mean free path of the carriers, and therefore, the application of pressure leads to enhancement of δl pinning mechanism. One can note that similar results have been reported in case of Fe$_x$NbSe$_2$[6,38], FeTe$_{0.7}$Se$_{0.3}$[61] and pnictides[34] superconducting compounds.

We have calculated the pinning force ($F_p = J_c H$) as a function of magnetic field under various hydrostatic pressures and have investigated the magnetic field dependence of the pinning force density (F_p) in order to understand vortex pinning mechanisms in this sample. Field dependence of F$_p$ [Fig. S4] for various temperatures in superconductors may be scaled into a unique curve if they are plotted as a function of reduced field, $h = H/H_{irr}$. The scaling of normalized pinning force from the Dew-Hughes formula[62], $f_p = h^p(1 - h)^q$, where p and q are the parameters describing the pinning mechanism. Further, $J_c^{0.5}H^{0.25}$ is plotted as a function of magnetic field is known as Kramer plot[63] and it is used to determine H_{irr}, where H_{irr} is determined as the extrapolated to zero field from various isotherms of J_c and the temperature dependent of H_{irr} shows a linear behavior.
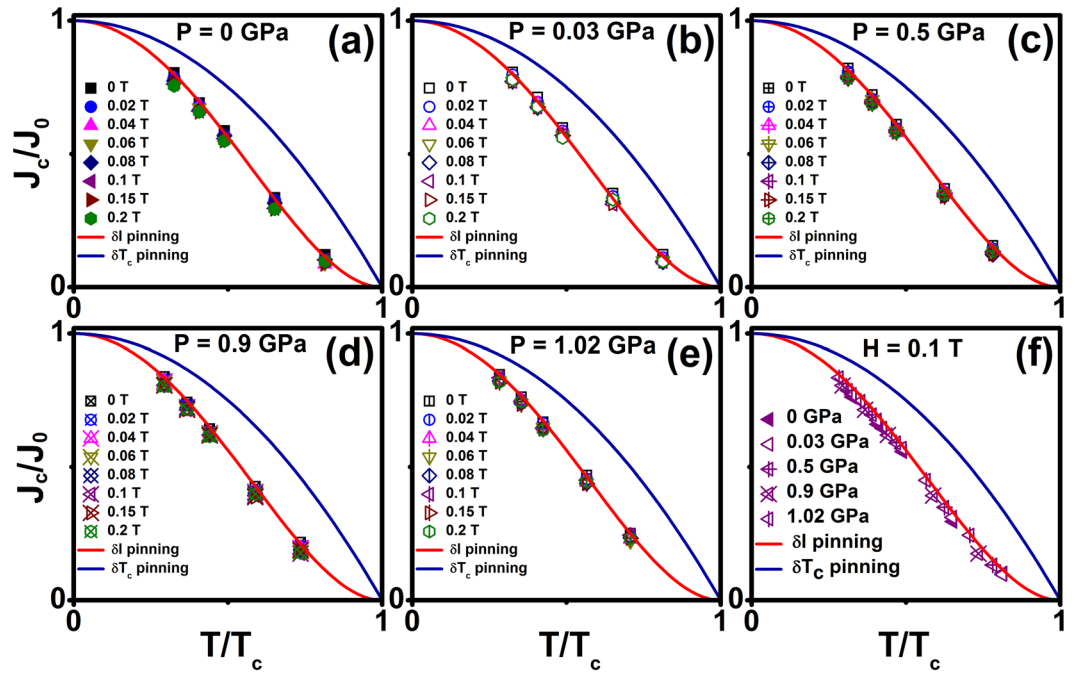
Figure 8. (a–f) Normalized J_c (J_c/J_0) as a function of reduced temperature (T/T_c) for various hydrostatic pressures on $Cr_{0.0005}NbSe_2$. The Solid line (red) is shown in δl pinning fitting and the solid line (blue) is shown in δT_c pinning fitting.
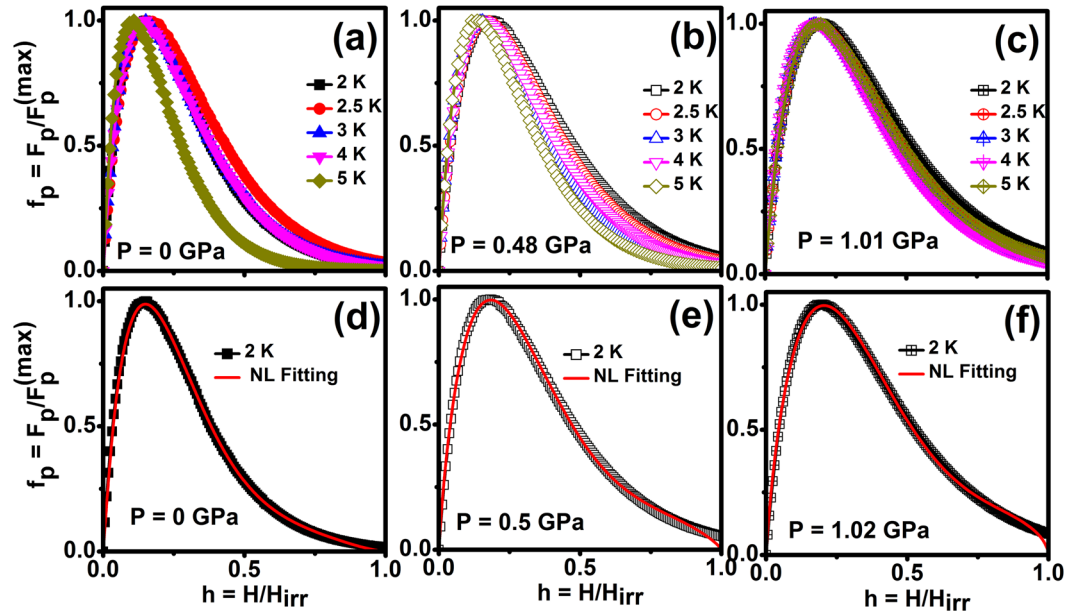

Figure 9. (a–f) Normalized pinning force density ($f_p = F_p/F_p^{(max)}$) as a function of reduced magnetic field ($h = H/H_{irr}$) for various hydrostatic pressures on $Cr_{0.0005}NbSe_2$. Solid lines are shown in the collective pinning model fitting at the log scale at a temperature of 2 K.

Figure 9(a–f) shows normalized pinning force ($f_p = F_p/F_p^{(max)}$) as a function of reduced critical field ($h = H/H_{irr}$) for various temperatures and constant P (0,0.5 and 1.02 GPa) [Fig. S5]. For the scaling of both point and surface pinning, we use the relation, $f_p = Ah^p(1-h)^q$, where p and q describes the nature of specific pinning mechanism[62]. It is known from Dew-Hughes model, when $p = 1/2$ and $q = 2$ and $p = 1$ and $q = 2$ describes the surface pinning and point pinning respectively as predicted by Kramer[63]. The best fit of the curves is obtained with $f_p(h)$ dependence given by, $h^{0.89}(1-h)^{4.38} + Bh^{0.72}(1-h)^{1.38}$ at 0 GPa and $h^{0.91}(1-h)^{5.70} + Bh^{0.79}(1-h)^{2.48}$ at 1.02 GPa. The application of pressure causes an increase of q parameter from 4.38 to 5.70 which is an indication of the increase of both pinning center and surface pinning mechanism. It reveals that the normal core point pinning

is more dominant than surface pinning mechanism under high pressure [Fig. S5]. The broadening of the pinning force with the application of pressure indicates that the pinning centers are enhanced with the application of pressure for this sample. Cr intercalation of into Se-Nb-Se layers of $NbSe_2$ single crystals leads to an increase of more pinning centers compared with the undoped $NbSe_2$.

Conclusion

In summary, we have shown that hydrostatic pressure is a very effective means to significantly enhance T_c, J_c, H_{irr}, and flux pinning in the $Cr_{0.0005}NbSe_2$ superconductor. We demonstrate that hydrostatic pressure significantly increases T_c from $M(T)$ ($dT_c/dP = 0.91$ K/GPa; $0 < P < 1$ GPa) and $\rho(T)$ (0.75 K/GPa; $P < 1.5$ GPa & 0.09 K/GPa; $1.5 < P < 8$ GPa) measurements. The pressure introduces more point defects in sample and it is responsible for enhancement J_c. We found that the hydrostatic pressure stabilizes a strong δl pinning mechanism. In addition, we found that the point pinning is more dominant than surface pinning under high pressure. The pressure enhanced the H_{c1}, H_{c2}, H_{irr} and reduces both coherence length and penetration depth which are responsible for the pinning mechanism.

Experimental Techniques

$Cr_{0.0005}NbSe_2$ single crystal has been synthesized using chemical vapour transport method. The essential commercially available high purity elemental metallic powders such as Nb (99.95%), Se (99.99%) and Cr (99.99%) procured from Alfa Aeser, which are mixed with suitable stoichiometric ratio and made of 6 mm (φ) pellet. The pellet kept in a sealed quartz tube with tiny amount of iodine in the presence of liquid nitrogen atmosphere. The sealed quartz tube is placed in a two-zone furnace with programmable temperature controller and the temperatures of charge and growth zone at 800 °C and 720 °C respectively for a period of seven days. The grown crystals are characterized structural phase and the elemental composition analyses are confirmed using x-ray diffraction and Energy dispersive X-ray Spectroscopy techniques respectively and further details about synthesis and characterization of these materials were recently reported by Rukshana Pervin et al.[64]. A cubic anvil pressure device, consisting of six tungsten carbide (WC) anvils, which have been used to produce homogeneous hydrostatic pressure up to 8 GPa for resistivity measurements[65]. The applied pressure is calibrated from the resistance changes of Bi with its phase transitions at room temperature such as Bi I-II (2.55 GPa), Bi II-III (2.77 GPa) Bi III'-V (7.68 GPa) and Daphne #7373 used as a pressure transmitting medium[66]. The temperature of sample inside the Teflon cell is monitored by measuring the resistivity of three calibrated Pt(Co) resistance thermometers attached to the neck of each anvil. The electrical contacts were made using gold wire of 20 μm φ and Ag paste is used to make contacts on the surface of the sample with the typical sample size is $0.8 \times 0.5 \times 0.5$ mm³. The standard four probe method is used for doing resistivity measurements under ambient and high pressure upto 8 GPa and the anvils are through the gold foil. The magnetic properties (ZFC & FC) of $Cr_{0.0005}NbSe_2$ single crystals were investigated under various magnetic fields at ambient and high pressures. The dc magnetization measurements under pressure were carried out using Physical Property Measurements System – Vibrating Sample Magnetometer (PPMS-VSM, Quantum Design, USA). The external pressure was generated up to ~1 GPa by a clamp type miniature hydrostatic pressure cell which is made of specially heat treated nonmagnetic Cu-Be alloy. The fluorinert FC #70 and FC #77 (1:1) mixture was used as a pressure transmitting medium and the *in-situ* pressure was estimated from the superconducting transition temperature of pure Sn which was loaded along with the sample in the capsule.

References

1. Shermadini, Z. *et al.* Coexistence of magnetism and superconductivity in the iron-based compound $Cs_{0.8}(FeSe_{0.98})_2$. *Phys. Rev. Lett.* **106**, 1–4 (2011).
2. Malliakas, C. D. & Kanatzidis, M. G. Nb-Nb interactions define the charge density wave structure of 2H-$NbSe_2$. *J. Am. Chem. Soc.* **135**, 1719–22 (2013).
3. Rice, T. M. & Scott, G. K. New Mechanism for a Charge-Density-Wave Instability. *Phys. Rev. Lett.* **35**, 117–120 (1975).
4. Frindt, R. F. Superconductivity in Ultrathin $NbSe_2$ Layers. *Phys. Rev. Lett.* **28**, 299–301 (1972).
5. Huang, C. L. *et al.* Experimental evidence for a two-gap structure of superconducting $NbSe_2$: A specific-heat study in external magnetic fields $NbSe_2$ (H) (mJ/mol K). *Phys. Rev. B* **76**, 212504 (2007).
6. Pervin, R. *et al.* Enhancement of superconducting critical current density by Fe impurity substitution in $NbSe_2$ single crystals and the vortex pinning mechanism. *Phys. Chem. Chem. Phys.* **19**, 11230–11238 (2017).
7. Xi, X. *et al.* Strongly enhanced charge-density-wave order in monolayer $NbSe_2$. *Nat. Nanotechnol.* **10**, 765–769 (2015).
8. Wilson, J. A., Di Salvo, F. J. & Mahajan, S. Charge-density waves in metallic, layered, transition-metal dichalcogenides. *Phys. Rev. Lett.* **32**, 882–885 (1974).
9. Chatterjee, U. *et al.* Emergence of coherence in the charge-density wave state of 2H-$NbSe_2$. *Nat. Commun.* **6**, 1–7 (2015).
10. Weber, F. *et al.* Extended phonon collapse and the origin of the charge-density wave in 2H-$NbSe_2$. *Phys. Rev. Lett.* **107**, 1–5 (2011).
11. Naik, I. & Rastogi, A. K. Transport properties of 2H-$NbSe_2$: Effect of Ga-intercalation. *Phys. B Condens. Matter* **405**, 955–957 (2010).
12. Luo, H. *et al.* S-Shaped Suppression of the Superconducting Transition Temperature in Cu-Intercalated $NbSe_2$. *Chem. Mater.* **29**, 3704–3712 (2017).
13. Zhang, X. *et al.* Magnetoresistivity plateau of graphene in proximity to superconducting $NbSe_2$. *Phys. Rev. B* **94**, 1–6 (2016).
14. Saito, Y., Nojima, T. & Iwasa, Y. Highly crystalline 2D superconductors. *Nat. Rev. Mater.* **2**, 16094 (2016).
15. Xi, X. *et al.* Ising pairing in superconducting $NbSe_2$ atomic layers. *Nat. Phys.* **12**, 139–143 (2016).
16. Brandt, E. H. The flux-line lattice in superconductors. *Rep. Prog. Phys.* **58**, 1465 (1995).
17. Ravikumar, G. *et al.* Stable and metastable vortex states and the first-order transition across the peak-effect region in weakly pinned $2H - NbSe_2$. *Phys. Rev. B - Condens. Matter Mater. Phys.* **63**, 1–8 (2001).
18. Zhou, W., Xing, X., Wu, W., Zhao, H. & Shi, Z. Second magnetization peak effect, vortex dynamics, and flux pinning in 112-type superconductor $Ca_{0.8}La_{0.2}Fe_{1-x}Co_xAs_2$. *Sci. Rep.* **6**, 1–10 (2016).
19. van der Beek, C. J. *et al.* Flux pinning in $PrFeAsO_{0.9}$ and $NdFeAsO_{0.9}F_{0.1}$ superconducting crystals. *Phys. Rev. B* **81**, 174517 (2010).
20. Blatter, G., Feigel'Man, M. V., Geshkenbein, V. B., Larkin, A. I. & Vinokur, V. M. Vortices in high-temperature superconductors. *Rev. Mod. Phys.* **66**, 1125–1388 (1994).
21. Nelson, D. R. Vortex Entanglement in High-Tc Superconductors. *Phys. Rev. Lett.* **60**, 1973–1976 (1988).
22. Nattermann, T. & Lipowsky, R. Vortex Behavior in High-T_c Superconductors with Disorder. *Phys. Rev. Lett.* **61**, 2508 (1988).

23. Yamamoto, A., Takeshita, N., Terakura, C. & Tokura, Y. High pressure effects revisited for the cuprate superconductor family with highest critical temperature. *Nat. Commun.* **6**, 1–7 (2015).

24. Xiao, Z. L., Dogru, O., Andrei, E. Y., Shuk, P. & Greenblatt, M. Observation of the vortex lattice spinodal in NbSe$_2$. *Phys. Rev. Lett.* **92**, 2–5 (2004).

25. Li, D. & Rosenstein, B. Melting of the vortex lattice in high-T$_c$ superconductors. *Phys. Rev. B* **65**, 220504 (2002).

26. Zeldov, E. *et al.* Thermodynamic observation of first order vortex-lattice melting transition in Bi$_2$Sr$_2$CaCu$_2$O$_8$. *Nature* **375**, 373 (1995).

27. Ishida, T., Okuda, K., Rykov, A. I. & Tajima, S. In-plane anisotropy of vortex-lattice melting in large single crystals. *Phys. Rev. B - Condens. Matter Mater. Phys.* **58**, 5222–5225 (1998).

28. Righi, E. F., Grigera, S. A., Nivea, G., Lopez, D. & de la Cruz, F. Finite vortex correlation in the c direction in YBa$_2$Cu$_3$O$_7$ above the first-order melting transition. *Phys. Rev. B* **55**, 14156–14159 (1997).

29. Liu, J., Li, S., Li, Y., Zhu, X. & Wen, H.-H. Pressure-tuned enhancement of superconductivity and change of ground state properties in LaO$_{0.5}$F$_{0.5}$BiSe$_2$ single crystals. *Phys. Rev. B* **90**, 094507 (2014).

30. Takahashi, H. *et al.* Superconductivity at 43 K in an iron-based layered compound LaO$_{1-x}$F$_x$FeAs. *Nature* **453**, 376–378 (2008).

31. Takahashi, H. *et al.* High-Pressure Studies on Superconducting Iron-Based LaFeAsO$_{1-x}$F$_x$, LaFePO and SrFe$_2$As$_2$. *J. Phys. Soc. Japan* **77**, 78–83 (2008).

32. Uehara, M. *et al.* Superconductivity in the Ladder Material Sr$_{0.4}$Ca$_{13.6}$Cu$_{24}$O$_{41.84}$. *J. Phys. Soc. Japan* **65**, 2764–2767 (1996).

33. Jung, S. G. *et al.* Enhanced critical current density in the pressure-induced magnetic state of the high-temperature superconductor FeSe. *Sci. Rep.* **5**, 1–7 (2015).

34. Shabbir, B. *et al.* Hydrostatic pressure: A very effective approach to significantly enhance critical current density in granular iron pnictide superconductors. *Sci. Rep.* **5**, 1–6 (2015).

35. Tomita, T., Schilling, J. S., Chen, L., Veal, B. W. & Claus, H. Enhancement of the critical current density of YBa$_2$Cu$_3$Ox superconductors under hydrostatic pressure. *Phys. Rev. Lett.* **96**, 7–10 (2006).

36. Jones, R. E., Shanks, H. R., Finnemore, D. K. & Morosin, B. Pressure effect on superconducting NbSe$_2$ and NbS$_2$. *Phys. Rev. B* **6**, 835–838 (1972).

37. Mattheiss, L. F. Energy bands for 2H-NbSe$_2$ and 2H-MoS$_2$. *Phys. Rev. Lett.* **30**, 784–787 (1973).

38. Manikandan, K. *et al.* Pressure assisted enhancement in superconducting properties of Fe substituted NbSe$_2$ single crystal. *Sci. Rep.* **8**, 1251 (2018).

39. Smith, T. F., Shelton, R. N. & Schwall, R. E. Pressure enhanced superconductivity in NbSe$_2$. *J. Phys. F Met. Phys.* **4**, 2009–2016 (1974).

40. Biletskyi, V. I., Chashka, K. B., Sokolov, A. N. & Vovk, R. V. The effect of high pressure on the electrical resistivity of 2H-NbSe$_2$ single crystals intercalated with deuterium. *Low Temp. Phys.* **41**, 514–516 (2015).

41. Suderow, H., Tissen, V. G., Brison, J. P., Martínez, J. L. & Vieira, S. Pressure induced effects on the fermi surface of superconducting 2H-NbSe$_2$. *Phys. Rev. Lett.* **95**, 2–5 (2005).

42. Grissonnanche, G. *et al.* Direct measurement of the upper critical field in cuprate superconductors. *Nat. Commun.* **5**, 1–8 (2014).

43. Mizuguchi, Y., Tomioka, F., Tsuda, S., Yamaguchi, T. & Takano, Y. Superconductivity at 27 K in tetragonal FeSe under high pressure. *Appl. Phys. Lett.* **93**, 2006–2009 (2008).

44. Okabe, H., Takeshita, N., Horigane, K., Muranaka, T. & Akimitsu, J. Pressure-induced high- Tc superconducting phase in FeSe: Correlation between anion height and T$_c$. *Phys. Rev. B* **81**, 1–6 (2010).

45. Bhoi, D. *et al.* Interplay of charge density wave and multiband superconductivity in 2H-Pd$_x$TaSe$_2$. *Sci. Rep.* **6**, 1–10 (2016).

46. Szabó, P. *et al.* Interlayer transport in the highly anisotropic misfit-layer superconductor (LaSe)$_{1.14}$(NbSe$_2$). *Phys. Rev. Lett.* **86**, 5990–5993 (2001).

47. Kasowski, R. V. Band Structure of MoS$_2$, and NbS$_2$. *Phys. Rev. Lett.* **30**, 1175–1178 (1995).

48. McMillan, W. L. Transition temperature of strong-coupled superconductors. *Phys. Rev.* **167**, 331–344 (1968).

49. Harper, J. M. E., Geballe, T. H. & DiSalvo, F. J. Thermal properties of layered transition-metal dichalcogenides at charge-density-wave transitions. *Phys. Rev. B* **15**, 2943–2951 (1977).

50. Le Tacon, M. *et al.* Inelastic X-ray scattering in YBa$_2$Cu$_3$O$_{6.6}$ reveals giant phonon anomalies and elastic central peak due to charge-density-wave formation. *Nat. Phys.* **10**, 52–58 (2013).

51. Zehetmayer, M. & Weber, H. W. Experimental evidence for a two-band superconducting state of NbSe$_2$ single crystals. *Phys. Rev. B* **82**, 1–5 (2010).

52. Werthamer, N. R., Helfand, E. & Hohenberg, P. C. Temperature and Purity Dependence of the Superconducting Critical Field, H$_{c2}$. III. Electron Spin and Spin-Orbit Effects. *Phys. Rev.* **147**, 295–302 (1966).

53. Brandt, E. H. Irreversible magnetization of pin-free type-ii superconductors. *Phys. Rev. B* **60**, 11939–11942 (1999).

54. Renosto, S. T. *et al.* Evidence of multiband behavior in the superconducting alloy Zr$_{0.96}$V$_{0.04}$B$_2$. *Phys. Rev. B* **87**, 1–6 (2013).

55. Bean, C. P. Magnetization of high-field superconductors. *Rev. Mod. Phys.* **36**, 31–39 (1964).

56. Bean, C. P. Magnetization of hard superconductors. *Phys. Rev. Lett.* **8**, 250–253 (1962).

57. Palau, A. *et al.* Simultaneous inductive determination of grain and intergrain critical current densities of YBa$_2$Cu$_3$O$_{7-x}$ coated conductors. *Appl. Phys. Lett.* **84**, 230–232 (2004).

58. Chen, Y. L. *et al.* Peak effect and superconducting properties of SmFeAsO$_{0.8}$F$_{0.2}$ wires. *Supercond. Sci. Technol.* **21**, 115014 (2008).

59. Yamamoto, A. *et al.* Small anisotropy, weak thermal fluctuations, and high field superconductivity in Co-doped iron pnictide Ba (Fe$_{1-x}$Co$_x$)$_2$As$_2$. *Appl. Phys. Lett.* **94**, 98–101 (2009).

60. Griessen, R. *et al.* Evidence for mean free path fluctuation induced pinning in YBa$_2$Cu$_3$O$_7$ and YBa$_2$Cu$_4$O$_8$ Films. *Phys. Rev. Lett.* **72**, 1910–1913 (1994).

61. Bonura, M., Giannini, E., Viennois, R. & Senatore, C. Temperature and time scaling of the peak-effect vortex configuration in FeTe$_{0.7}$Se$_{0.3}$. *Phys. Rev. B* **85**, 1–11 (2012).

62. Dewhughe., D. Flux pinning mechanisms in type-II superconductors. *Philos. Mag.* **30**, 293–305 (1974).

63. Kramer, E. J. Scaling laws for flux pinning in hard superconductors. *J. Appl. Phys.* **44**, 1360–1370 (1973).

64. Pervin, R., Manikandan, K., Rana, A. K., Arumugam, S. & Shirage, P. M. Effect of Cr atoms in vortex dynamics of NbSe$_2$ superconductor and study of second magnetization peak effect. *Mater. Res. Express* **7**, 076001 (2018).

65. Mori, N., Takahashi, H. & Takeshita, N. Low-temperature and high-pressure apparatus developed at ISSP, University of Tokyo. *High Press. Res.* **24**, 225–232 (2004).

66. Honda, F. *et al.* High-pressure apparatus for the measurement of thermal and transport properties at multi-extreme conditions. *J. Physics-Condensed Matter* **14**, 11501–11505 (2002).

Acknowledgements

Author Contributions

S.A. contributed for overall supervision of this work and involved in high pressure resistivity measurements in Cubic Press and magnetization measurements using PPMS-VSM, revision of manuscript. R.P. and P.M.S. synthesized the high quality of the Cr substituted $NbSe_2$ single crystals and carried out the structural measurement and analysis. M.K. conducted the magnetization measurements under hydrostatic pressure up to ~1 GPa using miniature piston cylinder pressure cell and also analyzed the data, wrote the manuscript. Y.U. involved in the high pressure electrical resistivity measurements in cubic press and the revision of the manuscript. K.I. and J.C. involved in high pressure electrical resistivity measurements up to ~8 GPa using cubic anvil pressure device. All authors contributed to the manuscript.

Additional Information

Supplementary information accompanies this paper at https://doi.org/10.1038/s41598-018-36672-x.

Competing Interests: The authors declare no competing interests.

Publisher's note: Springer Nature remains neutral with regard to jurisdictional claims in published maps and institutional affiliations.